Threshold Behavior in Electron-Transfer Collisions between Rubidium Atoms and C_2F_5Cl or C_2F_5I Molecules

Beike Jia, Sean Harris, Larry L. Lewis, Jiping Zhan, and Philip R. Brooks*

Chemistry Department and Rice Quantum Institute, Rice University, Houston, Texas 77251

Received: June 25, 2005; In Final Form: August 16, 2005

Rubidium atoms are accelerated in a high-temperature expansion of hydrogen to produce beams with energies high enough to observe collisional ionization with a cross beam. The speed of the atoms is directly measured by time-of-flight techniques, and the positive and negative ions produced are detected in separate mass spectrometers and detected in coincidence. Chloroperfluoroethane produces $C_2F_5^-$ and Cl^- ions, whereas iodoperfluoroethane produces I^-, $C_2F_5^-$, and $C_2F_5I^-$ ions. When the measured speed distributions are used, the signal versus energy may be deconvolved to yield thresholds and electron affinities (EAs). The EA for C_2F_5I is measured to be 0.96 ± 0.1 eV. Anomalously high EA values result for C_2F_5 apparently because $C_2F_5^-$ is produced by parts per million concentrations of Rb_2.

I. Introduction

Negative ions are common in solution and important in many biological processes, balancing positively charged species to maintain overall electroneutrality. But despite their importance and abundance, negative ions are far less well-characterized in the *gas phase* than are positive ions. This apparent discrimination arises because it is much easier to make positive ions than it is to make negative ions. Both are typically made by electron bombardment, but knocking out an electron (eq Ia) gives a strongly bound positive species (which frequently fragments), whereas the electron must attach itself to the molecule (eq Ib) to form a negative ion. The extra electron is weakly bound, and an attachment is likely only at "resonances".[1,2]

$$e^- + M \rightarrow M^+ + 2e^- \quad \text{(Ia)}$$

$$e^- + M \rightarrow M^- \quad \text{(Ib)}$$

The fate of a transient negative ion depends on the lifetime of the ion. The ion may autodetach the weakly bound electron with lifetimes ranging from milliseconds to femtoseconds, and this process can be studied by measuring the transmission of electrons through a gas. If the lifetime is long enough, one or more chemical bonds may break to produce a stable negative fragment and many radical ions can be produced and studied.[3] The stable parent negative ion cannot be produced unless a third body, such as a surface, another molecule, or a photon, is available to carry off the excess energy.

Electron-transfer collisions between heavy particles also produce negative ions, and these negative ions can be different from those produced by electron bombardment because the positive ion can carry away excess energy.[4,5] For example, SF_6 attaches electrons to form a metastable SF_6^- ion only at zero energy,[6] whereas SF_6^- (of unknown lifetime) can be observed at collision energies ≈ 20 eV with K atoms.[7] We exploit this difference to study electron-transfer collisions because these are more likely to serve as models for solution phase processes than is electron bombardment. We report here a preliminary study of the ions formed at the energetic threshold (Th) for the separation of ions and the measurement of the threshold energy. By definition, the threshold is that point where the signal vanishes, and we enhance the sensitivity by the coincidence counting of the product ions. High-beam intensities from seeded supersonic beams[8,9] further enhance the signals near the threshold and allow direct determination of the beam speed.

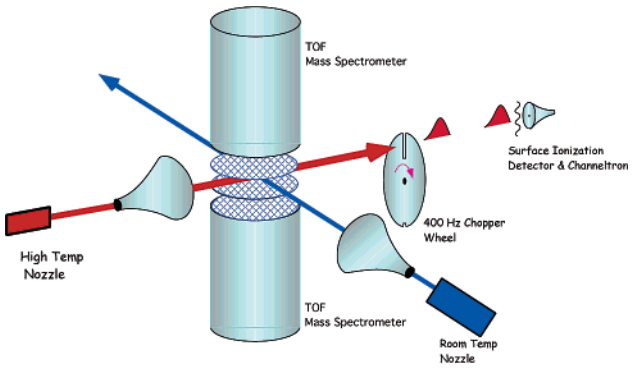

Figure 1. Schematic view of apparatus. Fast-atom beam crosses the molecular beam between the TOF mass spectrometers that detect ions formed in collision. Atomic speeds are measured by the flight time of packets of atoms produced by the chopper.

II. Experimental Section

Electron transfer between neutral species produces positive and negative ions. These can be separately detected if the energy available is enough to overcome the Coulomb attraction between the ions. In these experiments, energy is supplied by Rb atoms (≈0.1 Torr) seeded in a large excess (>99.9%) of hydrogen and expanded from a 0.002-in. diameter ruby nozzle at temperatures of ≈1100 K. Changing the backing pressure (from ∼400 to ∼1500 Torr) was the most convenient way to vary the energy.

The seeded atomic beam crosses a molecular beam at an angle of 120° in an apparatus sketched in Figure 1, slightly modified from one described earlier.[10−13] The molecular beam is nominally a 10% mixture of a test gas in argon or helium expanded through a 0.002-in. diameter ruby nozzle at room temperature. For C_2F_5I, the signal was too large for coincidence measurements, and it was necessary to dilute the gas to 0.03%. The backing pressure is held constant at 250 Torr in all experiments. The beams cross between two Wiley−McLaren[14] time-of-flight (TOF) mass spectrometers housed in an ultrahigh vacuum chamber.

* Corresponding author. E-mail: brooks@rice.edu.

10.1021/jp053460t CCC: $30.25
Published on Web 09/22/2005

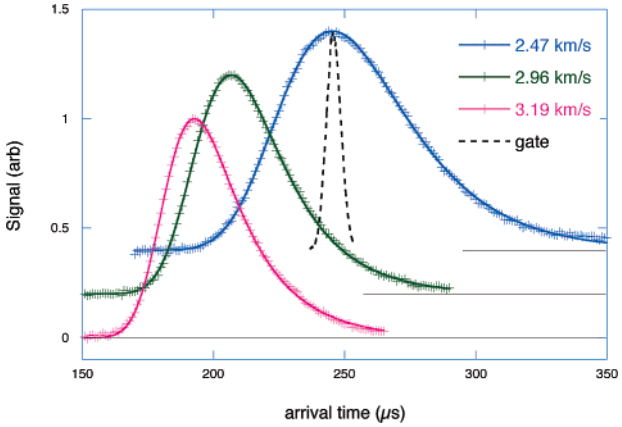

Figure 2. Arrival time distributions for Rb atoms at various H_2 pressures. Speeds are parameters of the curves passing through the experimental data (see text). The dashed curve is the gate function.

The beams are continuous and the mass spectrometer voltages are direct current, so there is no time zero. But, the ions are formed simultaneously by the electron transfer, and the unknown time zero is the same for both the positive ion and the negative ion. These ions are extracted perpendicular to the beam plane and are detected in separate and identical TOF mass spectrometers. Experiments and calculations showed that all of the ions are collected at the energies in these experiments. Because the positive ion is (almost certainly) Rb^+ and the distances and voltages are known, the *difference* in flight times is a measure of the mass of the negative ion. The ions are detected by microchannel plates (MCPs), and the electronic pulse from the positive ion detector is used to start a Lecroy 2228A time-to-digital converter (TDC), which has been modified to have a full-scale range of 10 μs. The pulse from the negative ion detector is delayed 4 μs, which stops the TDC, and the time *difference* is read by a computer. The delay ensures that all negative ions, including electrons, will arrive at the TDC after the start pulse. This design is simplified from that previously described for studying reactions of oriented molecules.[7]

III. Results

Speed Distributions. The beam is not monoenergetic, especially not in comparison to the electron beams in the electron bombardment experiments.[3] Because a moderate velocity dispersion of ≈10% translates into an energy dispersion of ≈20%, the signal will be a convolution over a large range of speeds, and it is necessary to accurately measure the speed distribution. The speed of the alkali beam is measured by time-of-flight: the beam is chopped into packets by a 400-Hz 3-in. diameter wheel containing a 0.015-in. slit through which the beam passes. A similar slit that is diametrically opposed interrupts the beam of an IR sensor to give a start signal, and the arrival time of the Rb atoms is monitored by a surface-ionization detector located $d = 563 \pm 2$ mm from the beam chopper. The atoms are ionized on a heated W wire, the ions are detected by a channeltron, and the pulse is digitized by an oscilloscope and recorded for later analysis.

Figure 2 shows typical arrival time distributions for Rb accelerated in H_2. Figure 2 also shows the open time of the chopper wheel, or the shutter function, $A(t)$, determined with a laser beam and a photomultiplier with a slit mask to mimic the detector wire.

Mass Spectra. Coincidence TOF mass spectra and arrival time distributions are obtained at each separate hydrogen backing pressure. Figure 3 shows typical mass spectra for Rb

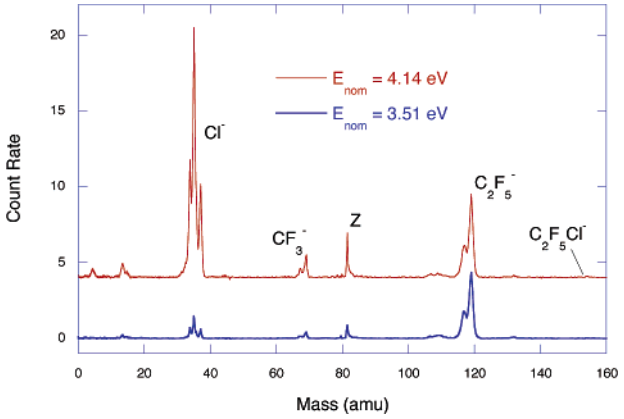

Figure 3. Coincidence TOF mass spectra showing negative ions formed by an electron transfer to C_2F_5Cl at two different energies. The high-energy spectrum is offset by 4 counts/s (cps).

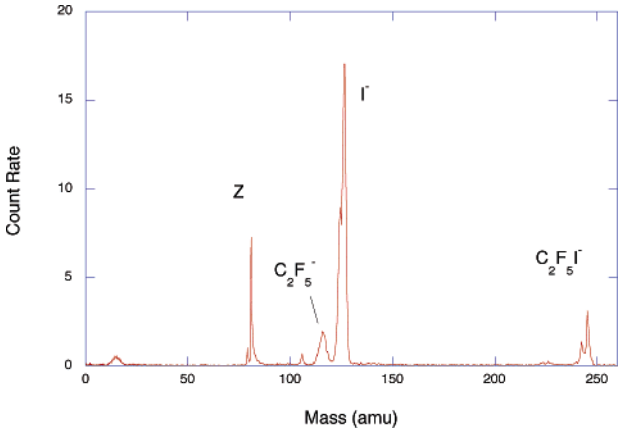

Figure 4. Coincidence TOF spectrum for C_2F_5I.

colliding with C_2F_5Cl at "high" and "low" backing pressures, corresponding to high and low energies.

Figure 3 is a *coincidence* spectrum: each mass peak is a consequence of the detection of two ions, a Rb^+ start pulse followed by a negative ion stop pulse. The unusual shape of the peaks (i.e., three apparent peaks for Cl^-) reflects the rubidium ion isotopes at $m/e = 85$ and 87, which account for 72 and 28% of the element[15] and give different "starts". The Cl^- peak should, thus, be a quartet; however, two of the lines strongly overlap, and we are able to resolve only three. The mass scale has been calibrated with several other gases such as CF_3Br and SF_6. The peak denoted "Z", the "zero-time peak", is an artifact apparently caused by a Rb^+ hitting the edge of a pore in the MCP and ejecting an electron backward to the negative ion detector, despite a grid in front of the MCP.[16] Because the electron moves so quickly, it is detected simultaneously with the positive ion, and a peak appears at zero time difference, corresponding to the mass of the alkali metal ion.

The difference between the two spectra in Figure 3 arises only from the difference in Rb speeds. Although the $C_2F_5^-$ intensity increases very slightly at higher energies, the Cl^- and CF_3^- intensities increase dramatically as if they had been suddenly turned on.

A representative mass spectrum for the analogous molecule C_2F_5I is shown in Figure 4; the situation is different from that of C_2F_5Cl. The $C_2F_5^-$ intensity is comparatively much lower, the I^- intensity is higher, and the intensity of the parent ion $C_2F_5I^-$ is much higher. For the iodide, the relative peak heights are essentially independent of the collision energy. The count rate for the two molecules is similar, but the chloride concentra-

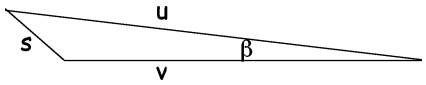

Figure 5. Velocity vectors for the collision of Rb with C_2F_5Cl.

TABLE 1: Speed Parameters

v_0 (km/s)	Δv (km/s)	τ_e (μs)
2.47	0.29	25
2.96	0.26	19
3.19	0.24	18

tion is ≈300 times higher, showing that the cross section for the iodide is about 300 times that of the chloride.

IV. Data Analysis

A. Rubidium Speed Distribution. A monoenergetic Rb beam of speed v would appear at the detector at a time $t = d/v$. In reality, the pulse of atoms is broadened by the finite temporal width of the chopper and by the distribution of speeds in the beam. The experimental arrival time distribution is, thus (see appendix I for details and nomenclature), a convolution of the speed distribution,

$$f_1(v) = B_1 v^2 \exp\left[-\left(\frac{v - v_0}{\Delta v}\right)^2\right] \quad (1)$$

together with the shutter function, $A(t)$, and any electronic response time, τ_e. The signal at the detector $S(t)$ is, thus,

$$S(t) = \int_0^t N(\tau) \exp\left(-\frac{t-\tau}{\tau_\epsilon}\right) d\tau = B_1 \int_0^t \exp\left(-\frac{t-\tau}{\tau_\epsilon}\right) d\tau \times \int_0^\tau A(\lambda) \frac{d^4}{(\tau-\lambda)^5} \exp\left[-\left(\frac{d}{\tau-\lambda\Delta v} - \frac{v_0}{\Delta v}\right)^2\right] d\lambda \quad (2)$$

Values of v_0 and Δv are varied in eq 2 and are compared to the experimental values using the Levenberg−Marquardt least-squares procedure[17] to find the values of v_0 and Δv that best fit the data. The solid lines in Figure 2 are calculated from these best-fit data. The agreement is excellent in virtually every case, and Figure 2 is truly *typical*. For illustration, Table 1 gives the values of v_0, Δv, and τ_e extracted from the data in Figure 2.

B. Relative Speed Distribution. The relative energy of collision is $^1/_2\mu u^2$, where μ is the reduced mass and u is the relative velocity. Because the Rb velocity is large compared to the velocity of the cross beam and the beams are crossed at 120° as shown in Figure 5, the relative velocity is mostly determined by v, the speed of Rb.

The speed of the gas beam, s, is approximated[18] as the stream velocity of a 10% mixture in He (793 m/s for C_2F_5Cl) with $s_0/\Delta s = 10$, and this assumed speed distribution is convolved with the measured Rb speed distribution to give a distribution of relative energies. Details of the calculations are in appendix II. This process is repeated for *each* energy point, and for illustration, Figure 6 shows relative collision energies from the speed-distribution parameters shown in Table 1 (obtained from the arrival time distributions of Figure 2). This figure also shows the "nominal" energy for each distribution, where the "nominal" energy for beams crossed at 120° is

$$2E_{nom} \equiv \mu u_0^2 = \mu(s_0^2 + v_0^2 + s_0 v_0) \quad (3)$$

Please note that energies higher and lower are present in the distribution.

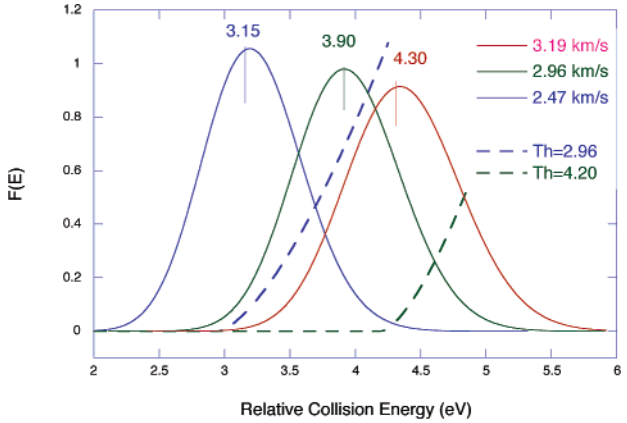

Figure 6. Relative collision energies calculated from the speed distribution parameters obtained from the arrival time distributions shown in Figure 2. *Nominal* collision energies are shown at the peak of each curve, but many collisions occur with energies up to 1 eV beyond the nominal value. The speed distribution of the gas beam is assumed to be given by an analogy to eq 1, with $s_0 = 793$ m/s and $\Delta s = 79$ m/s. Meier function thresholds are shown for 2.96 and 4.20 eV. See text for details.

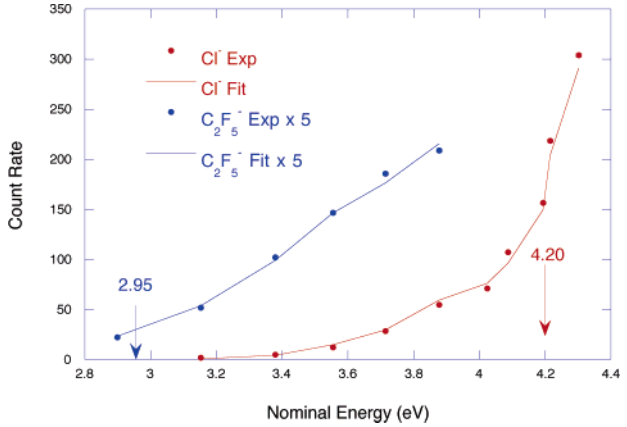

Figure 7. Signals for Cl^- and $C_2F_5^-$ arising from collisions of Rb and C_2F_5Cl at various nominal energies. Symbols are larger than error bars. Lines connect points calculated from a best fit of eq A19 using best-fit parameters and should not necessarily be smooth curves. Arrows denote thresholds obtained from these data; the thresholds in Table 2 are the average of several other determinations not shown.

C. Energy Thresholds. Integrated mass signals for C_2F_5Cl are shown in Figure 7 for various "nominal" collision energies, including those shown in Figure 6. Because the collision energy is not monoenergetic, it is necessary to convolve the energy distribution with the excitation function. For processes producing three particles, such as the ionizing reactions of eq 4, Maier[19] showed that the excitation function should have the form in eq 5

$$Rb + C_2F_5Cl \rightarrow Rb^+ + Cl^- + C_2F_5 \quad (4a)$$

$$Rb + C_2F_5Cl \rightarrow Rb^+ + Cl + C_2F_5^- \quad (4b)$$

$$E \le Th \qquad \sigma = 0$$
$$E > Th \qquad \sigma = \sigma_0(E - Th)^{3/2} \quad (5)$$

The Wigner step function[20] was used to deconvolve the threshold of $C_2F_5I^-$, where only two particles are formed. Threshold values were obtained by a nonlinear least-squares fit to the experimental data, as discussed in appendix III, with the results shown in Figure 7.

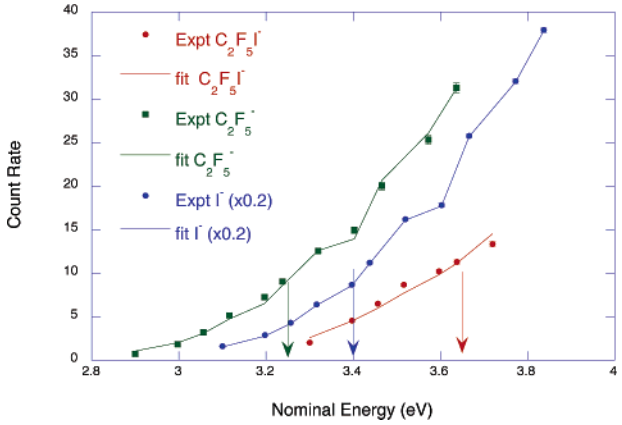

Figure 8. Experimental points and fit for ions from C_2F_5I. For clarity, experimental points and fits for I^- are shifted to higher energies by 0.2 eV, and those for $C_2F_5I^-$ are shifted by 0.4 eV. Most points are larger than the error bars; lines connect points calculated from eq A19 using best-fit parameters and should not necessarily be smooth curves. Arrows denote thresholds from these data; the thresholds in Table 2 are the average of several other determinations not shown.

The data shown in Figure 7 are taken at the same time, and the Rb speed distribution is measured at each "nominal" collision energy. The best-fit thresholds are clearly different for the two ions, and "nominal" energies below threshold still produce signal. This is understandable from Figure 6, which shows excitation functions for these data and thresholds. For a "nominal" energy of 3.90 eV, there is considerable overlap, with the excitation function having a threshold of 4.2 eV. The overlap at a nominal energy of 3.15 is far less, and the overlap in the wings of the distribution is sensitive to speeds that are not accurately measured. As a consequence, threshold determination is something of an iterative procedure: rough thresholds are determined, and then, the measurements are restricted to "nominal" energies, where $F(E)$ at the threshold was greater than ~0.1. For example, the experimental point with a nominal energy of 3.15 eV is not used to fit Cl^- because the high-speed tail is not well-known. Likewise, energies >3.9 eV are not considered for fitting $C_2F_5^-$ because the distribution of low energies is not well-known. At higher collision energies, the excitation function is no longer in the threshold regime, and these points are also excluded. The fit is calculated from eq A19 using the speed distribution for the Rb beam, $f_1(v)$, which is determined at each point. Eq A19 includes a term proportional to the beam flux, S_{ATD} (A17). This is measured at each point, and it is apparently slight variations in the beam flux that produce curves that are not smooth but which still fit the experiments.

The experiments represented in Figures 7 and 8 were repeated several times for both C_2F_5Cl and C_2F_5I. In a given experiment, the energy range was sometimes optimized only for one ion. Similar experiments were done on test gases such as CF_3Br and SF_6. These are summarized in Table 2.

V. Discussion

The energetic threshold (Th) for ion-pair formation is related to the electron affinity (EA) of the acceptor and the ionization potential (IP) of the donor by the relation

$$\text{Th} \geq \text{IP} - \text{EA} + \text{BDE} \qquad (6)$$

where BDE is the dissociation energy of any chemical bonds that must be broken to form the negative ion. The negative ion is likely to be formed in an excited state via a Franck−Condon process in which the electron is attached to the molecule in a time much less than that required for the nuclei to move to their (new) equilibrium positions. The inequality is necessary to account for any excess energy appearing either as internal or as translational energy of the products.

TABLE 2: Measured Thresholds[a]

molecule	ion	Th (eV)	EA (eV)	EA lit. (eV)
CF_3Br	Br^-	≈3.13 ± 0.1	≈4.12[b]	3.37[21]
	CF_3Br^-	3.25 ± 0.08	0.93 ± 0.08	0.91[22]
SF_6	SF_6^-	3.80	0.48	0.3−1.2[23]
C_2F_5Cl	Cl^-	4.27 ± 0.11	3.47 ± 0.13[c]	3.61[23]
	$C_2F_5^-$	2.93 ± 0.08	see text	≈2[23]
C_2F_5I	I^-	3.13 ± 0.08	3.27 ± .09[d]	3.06[23]
	$C_2F_5^-$	3.20 ± 0.09	see text	≈2[23]
	$C_2F_5I^-$	3.22 ± 0.03	0.96 ± .03	

[a] IP(Rb) = 4.18.[23] [b] BDE(C−Br) ≈ 3.06.[24] [c] BDE(C−Cl) ≈ 3.59.[24] [d] BDE(C−I) ≈ 2.22.[24]

Most of the EAs listed in Table 2 are in reasonably good agreement with literature values, except for Br and C_2F_5 (see below). The EA of C_2F_5I has apparently not been previously measured.

The discrepancy between our value for Br^- and the better-established literature value arises because the mass peaks for Br^- (m/e = 79 and 81) overlap the "zero-time peak" in the coincidence mass spectrum. This problem is worse at low-signal rates and, consequently, the threshold is strongly affected.

The EA for C_2F_5 has been omitted from Table 2 because we believe values calculated from our measured thresholds are not reliable. The threshold for $C_2F_5^-$ formed from C_2F_5Cl gives an EA = 4.84 eV, which is drastically different from previous measurements that were near 2.0 eV[25,26] and a theoretical value of 1.8 eV.[27] Iodoperfluoroethane was studied to give an independent determination of the threshold for $C_2F_5^-$, and its threshold yields a lower value for EA = 3.20 eV, which is still much greater than generally accepted.

A possible explanation for the widely varying EAs of C_2F_5 is that the $C_2F_5^-$ ion is being made in different states in the various experiments. In the present experiments, the Rb electron donor materially participates in the electron-transfer process, possibly deactivating the transient negative molecular ion and giving the adiabatic EA. But there is another possibility that we believe is more likely. Alkali metals are known to dimerize in the gas phase, and many spectroscopic properties[28] and reactivities[9,29−36] of the dimers are known. The dimers constitute about 0.1% of the alkali vapor above the liquid but dissociate upon heating the vapor independent from the liquid. (We estimate that, for equilibrium in the nozzle at 1100 K, the fraction of dimers in the Rb vapor is 10−100 ppm.) The coincidence mass spectra require a Rb^+ ion to start the clock; otherwise, the mass calibration would be vastly different. But the dimer could produce Rb^+ according to eq 7,

$$Rb_2 + C_2F_5X = Rb^+ + C_2F_5^- + RbX \qquad (7)$$

with Th = BDE(Rb_2) + IP(Rb) + BDE(C−Cl) − EA(C_2F_5) − BDE(RbX). When the values for BDE and IP in Table 2 and Huber and Herzberg's[28] BDE for Rb_2, RbCl, and RbI (0.49, 4.34, and 3.30 eV, respectively) are used, the threshold for reaction 7 is predicted to be 1.92 eV (C_2F_5Cl) and 1.59 eV (C_2F_5I), assuming EA(C_2F_5) = 2.0 eV.

The "threshold" reported in Table 2 for $C_2F_5^-$ from C_2F_5Cl is 2.9 eV, calculated for the reaction of the monomer, eq 4b. The speed of the Rb atom giving this collision energy is ≈2.4 km/s, which is considerably slower than the 4.6 km/s expected

TABLE 3: Tests for Dimer Participation in C_2F_5Cl

T_N (K)	T_B (K)	v_0 (km/s)	Δv (km/s)	Cl^- (cps)	$C_2F_5^-$ (cps)	$Cl^-/C_2F_5^-$
1091	498	3.02	0.33	63 ± 3	8 ± 0.4	7.8 ± 0.5
835	498	3.01	0.25	4.5 ± 0.1	3 ± 0.1	1.5 ± 0.06
1091	416	3.02	0.29	3.7 ± 0.1	0.21 ± 0.02	18 ± 2
1091	498	2.84	0.33	11 ± 0.5	5.4 ± 0.2	2 ± 0.1
835	498	2.84	0.26	1.1 ± 0.03	1.6 ± 0.05	0.7 ± 0.03

from eq A6 for the H_2 seed gas. The speed of the Rb dimer is not known but certainly lags behind the speed of the monomer. When a small-angle kinematic model for the acceleration of the monomer (appendix IV) is used, the measured speed of the monomer allows us to estimate the dimer speed at this "threshold" as ≈1.4 km/s. The nominal collision energy of the dimer at this speed is ≈1.6 eV, which is in rough agreement with the expected threshold for the reaction of the dimer. A similar calculation for the iodide suggests that the dimer energy at its "threshold" is ≈2.4 eV. Thus, the dimer has enough energy to react at the respective thresholds, but the energy of the dimer is less than the energy of the monomer.

The corresponding reaction of the dimer to produce Cl^-

$$Rb_2 + C_2F_5Cl = Rb^+ + Cl^- + RbC_2F_5 \qquad (8)$$

is highly unlikely because RbC_2F_5 is probably weakly bound, and the threshold for forming $Rb^+ + Cl^- + Rb + C_2F_5$ will be about 4.7 eV, corresponding to an apparent energy of the monomer ≈ 7 eV. Formation of Cl^- is, thus, dominated by the monomer reaction.

Two sets of auxiliary measurements were made to see if the Rb dimer played a role in the measurements. The experimental conditions and results for these tests are shown in Table 3. Decreasing the rubidium nozzle temperature from 1091 to 835 K and keeping the oven temperature at a constant 498 K should favor dimer formation by increasing the equilibrium constant, *K*, for the dimerization reaction. This temperature decrease had little effect on v_0, although Δv decreased a bit. Both the Cl^- and $C_2F_5^-$ signals decreased, but the $C_2F_5^-$ signal *increased* relative to the Cl^- signal as can be seen in the ratio. A similar result was obtained at a lower backing pressure (2.84 km/s). If atoms are responsible for both Cl^- and $C_2F_5^-$, the ratio should not change, but if dimers are responsible for $C_2F_5^-$, we expect lower nozzle temperatures to favor dimers and to decrease the signal ratio, as observed. In a second test, the oven temperature is lowered to 416 K, keeping the nozzle temperature at 1091 K. The equilibrium dimer pressure, P_D, is given by $P_D = KP_M^2$, where *K* is the equilibrium constant for dimerization and P_M is the monomer pressure. Decreasing the temperature drastically lowers the vapor pressure P_M, and the dimer pressure is expected to further decrease. Thus, if $C_2F_5^-$ arises from the dimer, decreasing the oven temperature should *lower* the $C_2F_5^-$ signal relative to Cl^- (the ratio should increase), and this is observed. We, thus, believe that the most likely explanation for our anomalously low threshold for $C_2F_5^-$ is that the ion is formed from the small (ppm) concentration of Rb dimers in the beam via eq 7. The numerical values for the $C_2F_5^-$ threshold are in error because we used the energy distribution for the monomer. Rough estimates of dimer speeds at the threshold are consistent with accepted values for the EA of C_2F_5 and further support the assignment of these thresholds to the dimer reaction, eq 7.

Electron attachment of iodoperfluoroethane, C_2F_5I, has been studied using monoenergetic electrons.[37] "Zero-energy" electrons produce I^-, and electrons a few volts higher produce F^- from several overlapping resonances. In the present experiments, we also observed I^-, but F^- was not observed because the energy was too low to break the C−F bond. As expected, the parent negative ion was observed in the electron-transfer experiments reported here but was not observed in the electron-attachment experiments. The EA of iodoperfluoroethane, C_2F_5I, is $0.96 \pm \sim 0.1$ eV and shows that this is a stable ion.

We believe this result is for the atomic reaction

$$Rb + C_2F_5I = Rb^+ + C_2F_5I^- \qquad (9)$$

The threshold for reaction 9 (Table 2) is apparently 3.22 eV, corresponding to a Rb speed of 2.46 km/s. Using the kinematic model of appendix IV, we estimate the dimer speed to be 1.46 km/s, giving a collision energy of the dimer as 2.4 eV. Possible dimer reactions are

$$Rb_2 + C_2F_5I = Rb^+ + C_2F_5I^- + Rb \qquad (10a)$$

$$Rb_2 + C_2F_5I = Rb_2^+ + C_2F_5I^- \qquad (10b)$$

The threshold for reaction 10a is ≈3.7 eV, higher even than the observed threshold and far higher than the estimated energy for the dimer, 2.4 eV. (Reaction 7 is much more exoergic than reaction 10a because the very stable RbCl is formed.) Reaction 10b produces a dimer ion that would give a totally different mass spectrum than what we observe, and it can be ruled out. We conclude that dimer channels do not complicate the determination of the threshold and that the parent negative ion, $C_2F_5I^-$, is produced from Rb atoms, as shown in reaction 9.

The EA of C_2F_5I, 0.96 ± 0.1 eV, is in reasonable agreement with other analogous halogen compounds: $EA(CF_3Br) = 0.91$ eV[22] and 0.93 eV (this work) and $EA(CF_3I) = 1.4$ eV[38] and 1.6 eV.[22] The $C_2F_5Cl^-$ ion appears in the mass spectrum as indicated in Figure 3, but the count rate was too small to enable us to analyze that peak.

VI. Summary

We have developed a heated supersonic source for producing atoms that are fast enough to cause collisional ionization in electron-transfer collisions. This source was used to accelerate rubidium atoms, and the intensity near threshold was high enough that we could directly and accurately measure the speed distribution at each separate collision energy.

The fast atoms cross a beam of molecules inside a coincidence TOF mass spectrometer that detects both positive and negative ions and uses the time difference between the ions as a signature of the mass. Molecules such as SF_6 and CF_3Br gave well-characterized ions. Using the measured speed distributions, we could *deconvolve* the intensity from the nominal energy to determine the Th for ion-pair formation and, thereby, determine EAs for various species.

Collisions of Rb with C_2F_5Cl produced Cl^- and $C_2F_5^-$ and initially suggested that the EA of C_2F_5 is greater than that for Cl^-. To further investigate this, C_2F_5I was examined, yielding a somewhat different value for C_2F_5 but, in addition, producing the parent negative ion, $C_2F_5I^-$. We believe the anomalous C_2F_5 results probably arise from $C_2F_5^-$, formed by minute amounts of Rb_2 in the beam.

We have measured the EA of C_2F_5I as 0.96 ± 0.1 eV.

Acknowledgment. We gratefully acknowledge support of this work over an extended period of time by the Robert A. Welch Foundation and the National Science Foundation.

Acknowledgment is made to the donors of the American Chemical Society Petroleum Research Fund for partial support of this research. B.J. gratefully thanks the Stauffer Foundation for a graduate fellowship.

Appendix I. Deconvolution of Speed Parameters

We assume the modified Maxwell−Boltzmann relation[39]

$$f_1(v) = B_1 v^2 \exp\left[-\left(\frac{v - v_0}{\Delta v}\right)^2\right] \quad \text{(A1)}$$

where v_0 is the stream velocity of the expansion, Δv is the measure of the deviation from the stream velocity, and B_1 is the normalization constant. The flight time, t, is given by $t = d/v$, and the distribution of flux arriving at the flux-sensitive detector at time t is

$$g(t) = v f_1(v) \left|\frac{dv}{dt}\right| = B_1\left(\frac{d^4}{t^5}\right) \exp\left[-\left(\frac{d/t - v_0}{\Delta v}\right)^2\right] \quad \text{(A2)}$$

This flux arriving at the detector is broadened by the finite open time of the chopper wheel that passes molecules as a function of time by presenting an open area $A(\lambda)$, measured using a laser and photomultiplier. $A(\lambda)$ is roughly a triangular function with full width at half-maximum $\approx 7\ \mu$s and is shown in Figure 2. A molecule passing through the chopper at time λ is detected at time τ, with the time zero as that time when a molecule first passes through the chopper. The speed is $v(\lambda,\tau) = d/(\tau - \lambda)$, and the number of molecules detected at time τ is

$$N(\tau) = \int_0^\tau g(\tau - \lambda)\, A(\lambda)\, d\lambda = B_1 \int_0^\tau A(\lambda) \frac{d^4}{(\tau - \lambda)^5} \times \exp\left\{-\left[\frac{d}{(\tau - \lambda)\Delta v} - \frac{v_0}{\Delta v}\right]^2\right\} d\lambda \quad \text{(A3)}$$

The electronic pulse is detected at time t, that is, delayed from τ by the exponential electronic response time τ_ϵ. This delay time is determined from the long-time tail of the arrival time distribution. The signal is finally detected at time t given by eq 2 from section IV, which is relabeled here as eq A4.

$$S(t) = \int_0^t N(\tau) \exp\left(-\frac{t - \tau}{\tau_\epsilon}\right) d\tau = B_1 \int_0^t \exp\left(-\frac{t - \tau}{\tau_\epsilon}\right) d\tau \times \int_0^\tau A(\lambda) \frac{d^4}{(\tau - \lambda)^5} \exp\left[-\left(\frac{d}{\tau - \lambda \Delta v} - \frac{v_0}{\Delta v}\right)^2\right] d\lambda \quad \text{(A4)}$$

These complications have been discussed by Young.[40]

Appendix II. Energy Distributions

Because neither beam is monoenergetic, the distribution of relative speeds is a convolution of the speeds in each beam. As shown in Figure 5, the Rb beam provides most of the energy, and the gas beam speed distribution is estimated as

$$f_2(s) = B_2 s^2 \exp\left[-\left(\frac{s - s_0}{\Delta s}\right)^2\right] \quad \text{(A5)}$$

where Δs is a measure of the deviation from the stream velocity, B_2 is the normalization constant, and s_0 is the constant stream velocity of a supersonic expansion, as approximated by

$$\frac{1}{2}\bar{m} s_0^{\,2} = \int_0^{T_0} \overline{C_P}\, dT \quad \text{(A6)}$$

Here, $\bar{m}$ is the average mass of the beam, T_0 is the nozzle temperature, and $\overline{C_P}$ is the average heat capacity of the beam. We assume $s_0/\Delta s \approx 10$, but this value is not critical.

From Figure 5, u is the relative collision speed, the beams cross at angle $\alpha = 120°$, and β, the angle between the velocity of the alkali metal **v** and the relative velocity **u**, ranges from 0 to 60°, depending on the relative magnitude of s and v. The relative velocity distribution $g(u,\beta)$ is given by

$$g(u,\beta)\, du\, d\beta = f_1(v)\, f_2(s)\, dv\, ds \quad \text{(A7)}$$

Integration over β gives the relative speed distribution.

$$f(u) = \int_0^{\pi/3} g(u,\beta)\, d\beta \quad \text{(A8)}$$

Substituting eqs A1 and A5 into eq A8 and following Datz et al.,[41]

$$\left(\frac{v - v_0}{\Delta v}\right)^2 + \left(\frac{s - s_0}{\Delta s}\right)^2 = \Omega^2 u^2 - \Phi u + \Gamma \quad \text{(A9)}$$

$$\Omega^2 = \left[\frac{\sin^2(\alpha + \beta)}{(\Delta v)^2} + \frac{\sin^2\beta}{(\Delta s)^2}\right]\frac{1}{\sin^2\alpha} \quad \text{(A10)}$$

$$\Phi = 2\left[\frac{v_0 \sin(\alpha + \beta)}{(\Delta v)^2} + \frac{s_0 \sin\beta}{(\Delta s)^2}\right]\frac{1}{\sin\alpha} \quad \text{(A11)}$$

$$\Gamma = \left(\frac{v_0}{\Delta v}\right)^2 + \left(\frac{s_0}{\Delta s}\right)^2 \quad \text{(A12)}$$

$$f(u) = \left(\frac{u}{\sin\alpha}\right)^5 \int_0^{\pi/3} \sin^2(\alpha + \beta) \sin^2\beta \times \exp[-(\Omega^2 u^2 - \Phi u + \Gamma)]\, d\beta \quad \text{(A13)}$$

Eq A13 is solved numerically, and the energy distribution is $F(E) = f(u)/\mu u$, where μ is the reduced mass.

Appendix III. Reaction Threshold

The rate S of a bimolecular chemical reaction is given by

$$S = V n_1^{\,0} n_2^{\,0} u \sigma(E) \quad \text{(A14)}$$

where $n_1^{\,0}$ and $n_2^{\,0}$ are the number densities of the reagents, V is the volume of the crossing region, $\sigma(E)$ is the energy-dependent reaction cross section, and u is the relative speed. The contribution to the rate from atoms with speeds in the range v to $v + dv$, and molecules with speeds in the range s to $s + ds$ is

$$d^2S = V\, dn_1(v)\, dn_2(s)\, u\sigma(E) = V B_2 n_1^{\,0} n_2^{\,0} u\sigma(E) \times B_1 f_1(v)\, f_2(s)\, ds\, dv = C B_1 n_1^{\,0} u\sigma(E)\, f_1(v)\, f_2(s)\, ds\, dv \quad \text{(A15)}$$

Because the source conditions of the molecular beam are constant throughout a given experiment, the normalization constants for beam 2 are combined with V to give the constant C.

Substituting eq A7 into eq A15, using the law of sines, and integrating, we have

$$S = C B_1 n_1^{\,0} \int_0^\infty u\sigma(E)\, f(u)\, du \quad \text{(A16)}$$

The arrival-time signal depends on the intensity of the Rb beam,

and the area under the arrival time distribution signal, S_{ATD}, is proportional to the total flux in the Rb beam. Thus,

$$S_{ATD} = \int V(t)\,dt = C_A B_1 n_1^0 \int v f_1(v)\,dv \qquad (A17)$$

where $V(t)$ is the voltage detected in the arrival time distribution measurements and

$$B_1 n_1^0 = \frac{S_{ATD}}{C_A \int v f_1(v)\,dv} \qquad (A18)$$

The final signal is, thus,

$$S = N \frac{S_{ATD}}{\int v f_1(v)\,dv} \int_0^\infty u\sigma(E)\, f(u)\,du \qquad (A19)$$

Eq A19 is evaluated using $f(u)$, obtained from eq A13, with the excitation function $\sigma(E)$ of eq 5. The unknown variables are the threshold, Th, and the scale factor N. These are extracted by using the Levenberg−Marquardt least-squares procedure[17] and by comparing the results to the experimental data.

Appendix IV. Estimate of Velocity Slip for Dimer

Figure 2 shows that the Rb atoms have a considerable velocity slip from the speed predicted by eq A6 for H_2, 4.6 km/s, and it is reasonable to expect that the dimer will be even slower. We can estimate the dimer speed from the *measured* monomer speed as follows:

Consider a collision between a fast, light particle (H_2) with mass m_L moving with speed v_L^0 and a slower heavy atom (Rb) of mass m_H moving with speed v_H^0, both moving in the x direction. Small-angle elastic collisions are most likely, and the Rb is accelerated by undergoing a large number, n, of very small angle, χ, collisions. The laboratory speed in the x direction after n such collisions is

$$v_H = v_H^0 + \frac{m_L}{2(m_L + m_H)}(v_L^0 - v_H^0) n\chi^2 \qquad (A20)$$

provided that $\chi \ll 1$ and that v_L is unchanged because the beam is >99.9% H_2.

From Table 2, the apparent $C_2F_5^-$ threshold is 2.9 eV, corresponding to $v_H \approx 2.4$ km/s, and eq A20 predicts that $n\chi^2 \approx 40$. If we assume that the dimer undergoes roughly the same number of small-angle collisions, eq A20 predicts that $v_{dimer} \approx 1.4$ km/s. The relative kinetic energy for the collision of the dimer with C_2F_5Cl is then estimated as 1.6 eV.

References and Notes

(1) Schulz, G. J. *Rev. Mod. Phys.* **1973**, *45*, 378.
(2) Schulz, G. J. *Rev. Mod. Phys.* **1973**, *45*, 423.
(3) Illenberger, E.; Momigny, J. *Gaseous Molecular Ions*; Springer-Verlag: New York, 1992.
(4) Nalley, S. J.; Compton, R. N.; Schweinler, H. C.; Anderson, V. E. *J. Chem. Phys.* **1973**, 4125.
(5) Tang, S. Y.; Rothe, E. W.; Reck, G. P. *Int. J. Mass Spectrom. Ion Phys.* **1974**, *14*, 79.
(6) Suess, L.; Parthasarathy, R.; Dunning, F. B. *J. Chem. Phys.* **2003**, *118*, 10919.
(7) Harris, S. A.; Wiediger, S. D.; Brooks, P. R. *J. Phys. Chem. A* **1999**, *103*, 10035.
(8) Bowen, K. H.; Liesegang, G. W.; Sanders, B. S.; Herschbach, D. R. *J. Phys. Chem.* **1983**, *87*, 557.
(9) Larsen, R. A.; Neoh, S. K.; Herschbach, D. R. *Rev. Sci. Instrum.* **1974**, *45*, 1511.
(10) Jia, B. Ph.D. Thesis, Rice University, Houston, TX, 2005.
(11) Maguire, T. C. Ph.D. Thesis, Rice University, Houston, TX, 1984.
(12) Barnes, M. D. Ph.D. Thesis, Rice University, Houston, TX, 1991.
(13) Maguire, T. C.; Brooks, P. R.; Curl, R. F.; Spence, J. H.; Ulvick, S. J. *J. Chem. Phys.* **1986**, *85*, 844.
(14) Wiley, W. C.; McLaren, I. H. *Rev. Sci. Instrum.* **1955**, *26*, 1150.
(15) Rosman, K. J. R.; Taylor, P. D. P. *Pure Appl. Chem.* **1998**, *70*, 217.
(16) Ma, C.; Sporleder, C. R.; Bonham, R. A. *Rev. Sci. Instrum.* **1991**, *62*, 909.
(17) Press, W. H.; Flannery, F. P.; Teukolsky, S. A.; Vetterling, W. T. *Numerical Recipes*; Cambridge University Press: Cambridge, MA, 1986.
(18) Abuaf, N.; Anderson, J. B.; Andres, R. P.; Fenn, J. B.; Marsden, D. G. H. *Science* **1967**, *155*, 997.
(19) Maier, W. B. *J. Chem. Phys.* **1964**, *41*, 2174.
(20) Wigner, E. P. *Phys. Rev.* **1948**, *73*, 1002.
(21) Blondel, C.; Cacciani, P.; Delsart, C.; Trainham, R. *Phys. Rev. A: At., Mol., Opt. Phys.* **1989**, *40*, 3698.
(22) Compton, R. N.; Reinhardt, P. W.; Cooper, C. D. *J. Chem. Phys.* **1978**, *68*, 4360.
(23) Linstrom, P. J., Mallard, W. G., Eds. NIST Standard Reference Database Number 69. *NIST Chemistry WebBook*; National Institute of Standards and Technology: Gaithersburg, MD, 2003.
(24) McMillen, D. F.; Golden, D. M. *Annu. Rev. Phys. Chem.* **1982**, *33*, 493.
(25) Harland, P. W.; Thynne, J. C. J. *Int. J. Mass Spectrom. Ion Phys.* **1972**, *9*, 253.
(26) Sullivan, S. A.; Beauchamp, J. L. *J. Am. Chem. Soc.* **1976**, *98*, 1160.
(27) King, R. A.; Pettigrew, N. D.; Schaefer, H. F. *J. Chem. Phys.* **1997**, *107*, 8536.
(28) Huber, K. P.; Herzberg, G. *Molecular Spectra and Molecular Structure. IV. Constants of Diatomic Molecules*; Van Nostrand Reinhold Company: New York, 1979.
(29) Baede, A. P. M.; Los, J. *Physica* **1971**, *52*, 422.
(30) Dispert, H.; Lacmann, K. *Chem. Phys. Lett.* **1977**, *47*, 533.
(31) Lin, S. M.; Mascord, D. J.; Grice, R. *Mol. Phys.* **1974**, *28*, 957.
(32) Reck, G. P.; Mathur, B. P.; Rothe, E. W. *J. Chem. Phys.* **1977**, *66*, 3847.
(33) Struve, W. S.; Krenos, J. R.; McFadden, D. L.; Herschbach, D. R. *J. Chem. Phys.* **1975**, *62*, 404.
(34) Wells, G. J.; Reck, G. P.; Rothe, E. W. *J. Chem. Phys.* **1980**, *73*, 1280.
(35) Whitehead, J. C.; Hardin, D. R.; Grice, R. *Mol. Phys.* **1973**, *25*, 515.
(36) Durham, M. A.; Marawar, R. W.; Lindsay, B. G.; Smith, K. A.; Dunning, F. B. *J. Chem. Phys.* **1992**, *96*, 7863.
(37) Langer, J.; Matejcik, S.; Illenberger, E. *Int. J. Mass Spectrom.* **2002**, *220*, 211.
(38) Tang, S. Y.; Mathur, B. P.; Rothe, E. W.; Reck, G. P. *J. Chem. Phys.* **1976**, *64*, 1270.
(39) Pauly, H. *Atom, Molecule, and Cluster Beams I*; Springer: Berlin, 2000; Vol. I.
(40) Young, W. S. *Rev. Sci. Instrum.* **1973**, *44*, 715.
(41) Datz, S.; Herschbach, D. R.; Taylor, E. H. *J. Chem. Phys.* **1961**, *35*, 1549.